

# Topology Design and Cross-layer Optimization for Wireless Body Sensor Networks

Yang Zhou<sup>a</sup>, Zhengguo Sheng<sup>b,\*</sup>, Chinmaya Mahapatra<sup>a</sup>, Victor C.M. Leung<sup>a</sup>,  
Peyman Servati<sup>a</sup>

<sup>a</sup>*Department of Electrical and Computer Engineering, the University of British Columbia,  
Vancouver, BC Canada V6T 1Z4*

<sup>b</sup>*Department of Engineering and Design, the University of Sussex, U.K. BN1 9RH*

---

## Abstract

Wireless Body Sensor Networks play a crucial role in digital health care nowadays. Due to the size limitation on the sensor nodes and the life critical characteristics of the signals, there are stringent requirements on network's reliability and energy efficiency. In this article, we propose a mathematical optimization problem that jointly considers network topology design and cross-layer optimization in WBSNs. We introduce multilevel primal and dual decomposition methods and manage to solve the proposed non-convex mixed-integer optimization problem. A solution with fast convergence rate based on binary search is provided. Simulation results have been supplemented to show that our proposed method yields much better performance than existing solutions.

*Keywords:* Wireless Body Sensor Network, network lifetime optimization, relay positioning

---

## 1. Introduction

Wireless Body Sensor Networks (WBSNs) are one of the key technologies that support the development of ubiquitous health care, which has attracted increasing attention in recent years. A typical WBSN is shown in Figure 1. The

---

\*Corresponding author

*Email addresses:* yangzhou@ece.ubc.ca (Yang Zhou), z.sheng@sussex.ac.uk (Zhengguo Sheng), chinmaya@ece.ubc.ca (Chinmaya Mahapatra), vleung@ece.ubc.ca (Victor C.M. Leung), peymans@ece.ubc.ca (Peyman Servati)

5 sensor nodes of WBSNs are either worn on or implanted in the human body. Though WBSNs have much shorter communication range and smaller scale than traditional Wireless Sensor Networks (WSNs), the channel environment is more severe for WBSNs. For example, for communication on the surface of human body, the performance will be seriously affected by temporal and spatial deep fading due to body movement, absorption and multipath effect of surrounding environment [1, 2, 3]. Observed from real-life data set [4], it can be concluded that the range and speed of on-body channel fluctuation are much larger for WBSNs than traditional WSNs. Moreover, propagation of implanted nodes' signals, on the other hand, will suffer from significant attenuation when signals go through various tissues and organs [5], and even greater challenges exist because of the complexity and variation of body tissues.

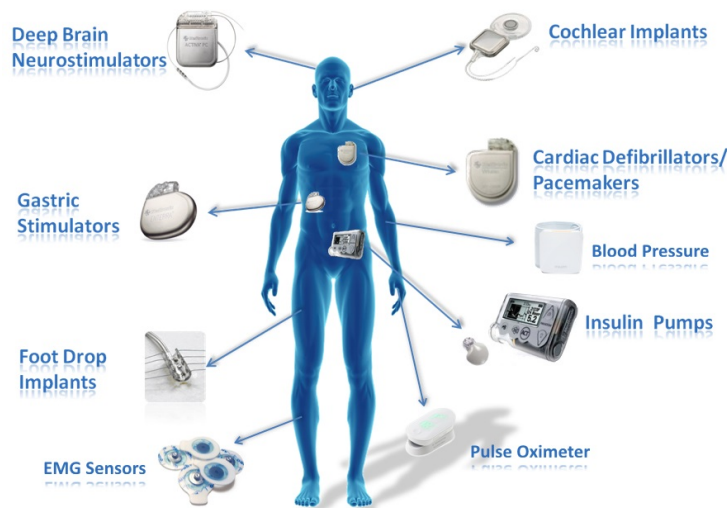


Figure 1: WBSN example

Energy efficiency is more crucial in WBSN than that is in traditional WSNs, since sensor nodes are of smaller size in order to be wearable and implantable. Their batteries are not likely to be replaced very often, especially for the implantable sensors. Reliability and latency performance need to be assured because the signals transmitted can be life critical. For certain WBSNs, emergency

situations and priority issues need also be handled properly.

The relay nodes are deployed, in order to prolong the network lifetime while ensuring the reliable data transmission with the required data rate. Relays can shorten the transmission range of the sensor nodes so that the sensor nodes are able to transmit with lower transmission power and with higher data rate. In this paper, we focus on how to prolong the lifetime of Wireless In-Body Sensor Networks. Specifically, we jointly consider the optimal locations of the relay nodes placed on the body surface, and the optimal transmission power and transmission time of the implanted sensors to achieve the maximum network lifetime. The decision of the optimal data routing on the routing layer, and the decision of transmission power and transmission time control on the physical layer are considered simultaneously. It can be seen further from problem model (4) that the considerations in these two layers cannot be decoupled. We formulate this problem as a mixed integer non-convex optimization problem which can be solved by the proposed multilevel primal and dual decomposition approach.

The remainder of the paper is organized as follows. Section II is the literature review on network optimization of WSNs and WBSNs. In Section III, we formulate the proposed cross-layer optimization problem and in Section IV, we describe our decomposition methods. A solution based on binary search for the optimal parameters with fast convergence rate is provided in Section V. The simulation results are presented in Section VI and Section VII concludes the paper.

## 2. Literature Review

As in [6, 7], the standard in use for the existing wearable medical devices are just the scaled down version of wireless technologies such as Bluetooth and WiFi. Little consideration is given to the peculiar characteristics of the human body. There are many optimization literatures for Wireless Sensor Networks (WSNs) [8, 9, 10, 11, 12, 13, 14]. However WBSNs have certain unique properties so that the conclusions for general WSNs may not be applied in WBSNs. According

to [15], the energy constraint for WBSNs is even harsher than that of WSNs because the volume of on-body or in-body sensor nodes needs to be tiny and the sensors are hard to be recharged generally. Since excessive radiation absorption will cause damages to the vulnerable body tissues, the transmission power of the sensor nodes and relay nodes need to be constrained. Furthermore, the body channels are highly unstable because of the irregularity of people's movements and the signal absorption incurred by body tissues. All of these constraints in WBSNs make data transmissions hardly reliable.

In order to deal with unstable channel status, relay has been proposed as one of the solutions in [15]. In [16, 17], the authors consider using relays to improve the network performance. According to simulation results, relays can reduce the outage rate and power consumption effectively. However, the decision of relay locations, which has profound influence on the performance, has not been discussed. In [18], an Energy-Aware WBSN Design Model (EAWD) is proposed to address the on-body relay positioning problem. However, only network layer is considered and no cross-layer design is included, which undermines its effectiveness in prolonging network lifetime. Furthermore, the proposed objective is minimizing total energy consumption and may lead to energy shortage for the heavily used nodes quickly.

In [19], the authors propose solutions to the energy minimization problem and network lifetime maximization problem based on intelligent time and power resource allocation in WBSN context. Both problems are formulated and solved as geometric programming. The network in [19] is single-hop star topology, where each node communicates directly with the coordinator. This proposed design is not proper for In-Body Sensor Networks since the transmission power of the implanted sensor nodes needs to be extremely low for both energy saving and body tissue protection. The star topology is not reliable enough considering the channel fluctuation around human body. Furthermore, since relay nodes can decrease the transmission power of sensor nodes by shortening the transmission distance, the network lifetime can be greatly prolonged by deploying relays.

In [20], the authors propose a relay based routing protocol for Wireless In-

Body Sensor Network. Network lifetime maximization and end-to-end-delay minimization problems are formulated and solved with linear programming. However, no systematical scheme is proposed to address the optimal relay location consideration. Furthermore, since the model proposed only considers routing layer, it fails to formulate a cross-layer optimization problem. Considerations on other layers, such as power control technique, are neglected.

### 3. System Model and Problem Formulation

We consider a Wireless Body Sensor Network with in-body sensors. The locations of the sensors are decided by doctors according to the patient's health status. The sensor set is represented by  $S$ . The relays locate on the surface of human body. For example, they can be worn on the clothes. The potential locations of on-body relay nodes are called the Candidate Sites (CSs) as in [21, 18]. The relay CS set is represented by  $R$ . A decision variable  $z_j, j \in R$  is used to denote whether a relay CS is chosen.  $z_j = 1$  represents that the  $j^{th}$  location of the relay CSs is used. Notations used are explained in Table 1. Figure 2a gives a quick view of the WBSN we consider. Grey dots represent the implanted sensor nodes. The blue crosses represent the relay CSs. The red star represents the coordinator. Each node is labelled with an ID, which is used in the simulation.

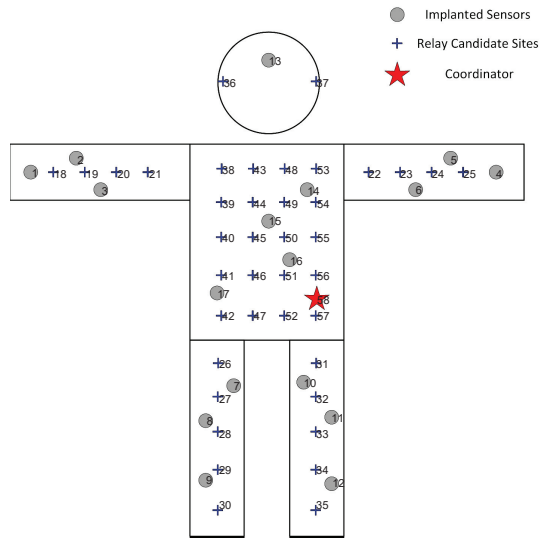
We divide the human body into six regions: left arm, right arm, left leg, right leg, head and torso. The node sets in each region, which include both implanted sensors and relay candidate sites, are denoted as  $G_1, G_2, G_3, G_4, G_5$  and  $G_6$ . Define total node set  $G = \{G_1, G_2, G_3, G_4, G_5, G_6\}$ .

Specifically, we consider the following scenario:

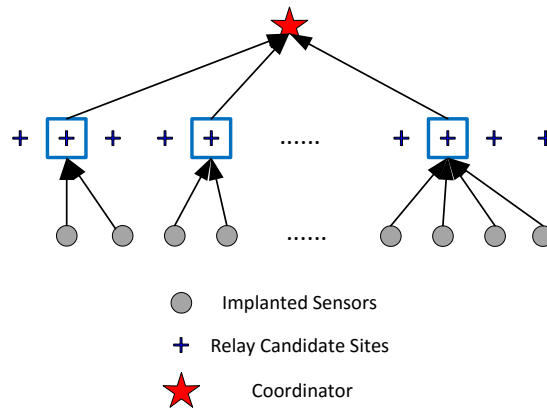
- The sensor nodes only utilize the relay CSs that are in the same body region, which will result in a stable network topology and communication performance. Though the relative distance among the nodes in different regions fluctuates significantly during the process of body movements, the relative distance among the nodes in the same region will be much less

Table 1: Notation Definition

Notation	Meaning
$S$	Sensor node set
$R$	Set of relay candidate sites
$c$	Coordinator
$L_i$	Lifetime for node $i$
$T_i$	Transmission time for node $i$ per superframe
$T_{frame}$	Duration of a superframe
$B_i$	Initial battery level for sensor node $i$
$r_{ij}$	Channel capacity for link $(i, j)$
$P_i$	Transmission power for sensor node $i$
$z_j$	Decision variable for relay candidate site $j$
$x_i$	Data generation rate for sensor node $i$
$G_k$	Node set in each body region
$G$	Total node set of all body regions
$P_{max}$	Maximum transmission power for each node
$P_{min}$	Minimum transmission power for each node



(a) WBSN nodes



(b) WBSN topology

Figure 2: WBSN nodes and topology

affected. So the requirement that each sensor only communicates with the relays in the same body region indicates that the data transmission of the sensors will remain stable. The relays are equipped with larger battery volume and are with higher transmission power, which are less sensitive to the distance fluctuation. Based on this consideration, a static network,

where the distance among the nodes is fixed, is assumed as in [20].

- The positions of the relay candidate sites are chosen depending on the locations of the implanted sensors, which are decided by the patient's actual health condition in the real application. Only the body regions with sensors implanted should contain relay candidate sites. In this article, it is assumed that the patient has randomly placed implanted sensors in each body region. In order to figure out the optimal places for the relays in the body regions, each body region is divided by grid with proper grid line spacing. The relay candidate sites are placed at the intersections of the grid. A grid with too large spacing may lead to inaccurate positions, and too small spacing will cause unnecessarily high computational complexity and little accuracy improvement. The grid line spacing used in this article turns out to be a good balance between complexity and accuracy, which results in reasonable simulation time consumption and good network performance.
- For each body region, only one relay is used. As the number of relays increases, the performance will improve. However, according to [22], the absorption of radiation will increase the temperature of body tissues. This can cause damage to sensitive organs by reducing the blood flow and growing certain type of bacteria. Because of the health consideration, the number of relays applied need to be low. The optimal number of relays to place is out of the scope of this article and it is assumed that only one relay is used in each region.
- Relays are placed on-body and they can be easily replaced or recharged compared with the implanted sensors. Thus as in [20], we do not include the considerations on relay's energy consumption and assume the relay nodes always transmit with the highest transmission power permitted.
- Multi-hopping among in-body sensors is not allowed and the in-body sensors transmit directly to the relays. The relay nodes transmit their data

145 directly to the coordinator as well since they have a high transmission  
 power. Thus the whole network is of a two-layer tree topology as is shown  
 in Figure 2b. The blue boxes represent the selected relay CS locations.

- As suggested by standard IEEE 802.15.6 protocol [23] that is widely used  
 by WBSN designs, TDMA scheme is adopted. Among all the nodes in  
 150 WBSN, each node transmits in its protected time slot and no other nodes  
 transmit simultaneously. Thus there is no interference among the trans-  
 missions.

Both IEEE 802.15.4 and IEEE 802.15.6, which are widely adopted by WB-  
 SNs, suggest Beacon-enabled TDMA scheme. A typical TDMA superframe  
 155 structure is shown in Figure 3. The superframe is composed of beacon frame,  
 Contention Free Period (CFP) and Inactive Period (IP). At the beginning of  
 each superframe, a beacon frame will be broadcasted to all nodes. The bea-  
 con frame contains the information for synchronization and resource allocation.  
 CFP is composed of Guaranteed Time Slots (GTSs) and is used for periodic  
 data transmission. During IP, all sensor nodes will turn off their radios and  
 160 sleep for energy saving.

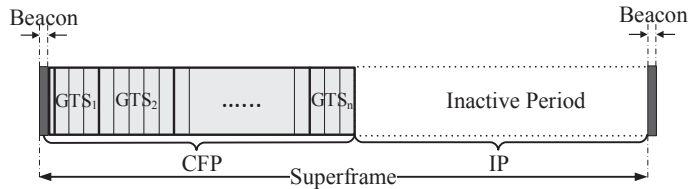


Figure 3: Superframe structure

Since there is no interference, the channel capacity  $r_{ij}$  can be expressed as  
 a function of  $P_i$

$$r_{ij} = W \log \left( 1 + \frac{\alpha_{ij} P_i}{N_j} \right) \quad (1)$$

where the base of the logarithmic function is 2,  $W$  is the bandwidth,  $N_j$  is the  
 power of noise and  $\alpha_{ij}$  is the channel gain between node  $i$  and  $j$ .

The network lifetime is defined as the duration until the first node of entire  
 165 body runs out of energy, which has been adopted in [24]. This definition is a  
 reasonable choice for WBSN. If some node dies, the whole WBSN can no longer  
 function well and guarantee the patient's safety because some critical health  
 information may be lost.

For each node, its lifetime can be calculated as

$$L_i = \frac{B_i}{P_i T_i / T_{frame}} = \frac{B_i T_{frame}}{P_i T_i} \quad (2)$$

The network lifetime is

$$\min_{i \in S} L_i = \min_{i \in S} \frac{B_i T_{frame}}{P_i T_i} \quad (3)$$

The locations of the relay candidates sites, the sensor nodes and the coordi-  
 170 nator are described by two dimensional coordinates in a reference system that  
 contains the human body shape. The distance among the nodes and hence the  
 path loss are calculated based on these coordinates.

We focus on maximizing the network lifetime by jointly considering the trans-  
 mission power ( $P_i$ ), transmission time ( $T_i$ ) and relay location decisions ( $z_j$ ). An  
 175 offline approach is proposed to derive these optimal network parameters. The  
 proposed model is defined as

$$\underset{P, T, z}{\text{maximize}} \quad \min_{i \in S} \frac{B_i T_{frame}}{P_i T_i} \quad (4a)$$

$$\text{subject to} \quad \sum_{i \in S} T_i + \sum_{j \in R} T_j z_j \leq T_{frame} \quad (4b)$$

$$T_i \sum_{j \in G_k \cap R} r_{ij} z_j \geq x_i T_{frame}, \quad i \in G_k \cap S, \quad G_k \in G \quad (4c)$$

$$\sum_{j \in G_k \cap R} r_{jc} T_j z_j \geq \sum_{i \in G_k \cap S} \sum_{j \in G_k \cap R} T_i r_{ij} z_j, \quad G_k \in G \quad (4d)$$

$$\sum_{j \in G_k \cap R} z_j = 1, \quad G_k \in G \quad (4e)$$

$$P_{\min} \leq P_i \leq P_{\max}, \quad i \in S \quad (4f)$$

$$z_j \in \{0, 1\}, \quad j \in R \quad (4g)$$

where objective function (4a) represents that the goal of the proposed algorithm is to maximize the network lifetime. Since TDMA-based scheme and superframe is adopted, all nodes will transmit their data periodically round by round. For inequality (4b), it states that the sum of the transmission time assigned to each node must be less than the time range of a superframe, which is the total time for a round of transmissions. Here we consider the situation that no time slot reuse is applied, which means no two nodes are allowed to transmit simultaneously or collision will happen. For inequality (4c), the flow balance of each sensor node  $i$  is considered. The data transmission speed of a sensor node need to be larger than the speed of its data generation.  $x_i$  is the average data generating speed for sensor node  $i$ .  $r_{ij}$  is the channel capacity and represents the maximum data rate possible between the sensor  $i$  and relay  $j$ . Note here only one relay  $j$  can be chosen in each body region  $G_k$ , which is constrained by (4e). For inequality (4d), similar to (4c), it describes the flow balance requirement for the relay nodes. If a relay candidate site  $j$  is used for body region  $G_k$ , then its output data rate to the coordinator need to be larger than the input data stream, which is the sum of all sensors' data stream in that region. If the relay candidate site  $j$  is not chosen,  $z_j$  would be 0, this inequality does not constrain anything. (4e) forces that within each body region, only one relay CS is chosen and actually used to install the relay. (4f) sets the lower and upper bounds on the transmission power of the sensor nodes. (4g) requires that the value of the decision variable  $z_j$  is limited to  $\{0, 1\}$ .

It is worth noting that (4c)-(4e) and (4g) are the constraints that state which relay to use for the data transmission of each sensor and it is a routing layer consideration. (4b) and (4f) are the constraints that state the transmission power and how much time is assigned to each sensor node in each superframe, which is a physical layer consideration. The physical layer and routing layer considerations are correlated since  $z$  appears in (4b)-(4e), and data rate  $r_{ij}$  in (4c)-(4d) is a function of power  $P_i$  in (4f). So the proposed problem is a cross layer problem that needs to be solved on physical layer and routing layer simultaneously.

#### 4. Multilevel Primal and Dual Decomposition Algorithm

The proposed problem (4) is not a convex problem. One difficulty results from the multiplication with the integer variable  $z_j$ , which makes (4b)-(4d) not convex. So the optimal solution of (4) cannot be solved directly. Therefore, we propose to use multilevel decomposition techniques and transform the original problem into several mixed integer sub-problems. Each sub-problem is confined within a body region and the optimal relay location can be derived by exhaustive search. Specifically, for a sub-problem in a certain body region, each relay CS will be tested and the one with the best objective function value will be selected. With decision variable  $z$  obtained first, the proposed problem can be solved.

##### 4.1. Decomposition Algorithm

By introducing a new variable  $t = \min_{i \in S} \frac{B_i T_{frame}}{P_i T_i}$ , (4a) can be replaced by  $t$ . A new constraint should be added as

$$t \leq \frac{B_i T_{frame}}{P_i T_i}, \quad i \in S \quad (5)$$

By using (4c), inequality (4d) can be transformed as

$$\sum_{j \in G_k \cap R} r_{jc} T_j z_j \geq \sum_{i \in G_k \cap S} T_i \sum_{j \in G_k \cap R} r_{ij} z_j \geq \sum_{i \in G_k \cap S} x_i T_{frame} \quad (6)$$

Apply log transformation to the variables with base  $e$  as  $\tilde{t} = \ln t$ ,  $\tilde{P}_i = \ln P_i$ ,

$\tilde{T}_i = \ln T_i$  and the original problem can be transformed into

$$\underset{\tilde{P}, \tilde{T}, \tilde{t}, z}{\text{maximize}} \quad \tilde{t} \quad (7a)$$

$$\text{subject to} \quad \tilde{t} + \tilde{P}_i + \tilde{T}_i \leq \ln(T_{frame} B_i), \quad i \in S \quad (7b)$$

$$\sum_{i \in S} e^{\tilde{T}_i} + \sum_{j \in R} e^{\tilde{T}_j} z_j \leq T_{frame} \quad (7c)$$

$$\tilde{T}_i + \ln \left( \sum_{j \in G_k \cap R} W \log \left( 1 + \frac{\alpha_{ij} e^{\tilde{P}_i}}{N_j} \right) z_j \right) \geq \ln(x_i T_{frame})$$

$$, \quad i \in G_k \cap S, \quad G_k \in G \quad (7d)$$

$$\ln \left( \sum_{j \in G_k \cap R} r_{jc} e^{\tilde{T}_j} z_j \right) \geq \ln \left( \sum_{i \in G_k \cap S} x_i T_{frame} \right), \quad G_k \in G \quad (7e)$$

$$\sum_{j \in G_k \cap R} z_j = 1, \quad G_k \in G \quad (7f)$$

$$\tilde{P}_{\min} \leq \tilde{P}_i \leq \tilde{P}_{\max}, \quad i \in S \quad (7g)$$

$$z_j \in \{0, 1\}, \quad j \in R \quad (7h)$$

Because of the coupling variable  $\tilde{t}$  in (7a)-(7b) and coupling constraint (7c), the problem is still central and cannot be solved locally in each body region. To mitigate the coupling effect of (7c), the Lagrangian of problem (7) is considered as

$$L(\tilde{t}, \tilde{T}, \tilde{P}, z, \lambda) = \tilde{t} - \lambda \left( \sum_{i \in S} e^{\tilde{T}_i} + \sum_{j \in R} e^{\tilde{T}_j} z_j - T_{frame} \right) \quad (8)$$

The Lagrange dual function  $g(\lambda)$  can be obtained from

$$\underset{\tilde{P}, \tilde{T}, \tilde{t}, z}{\text{maximize}} \quad L(\tilde{t}, \tilde{T}, \tilde{P}, z, \lambda) \quad (9)$$

$$\text{subject to} \quad (7b), (7d) - (7h)$$

If we call problem (7) as the master problem, the dual problem of the master problem is

$$\underset{\lambda}{\text{minimize}} \quad g(\lambda) \quad (10a)$$

$$\text{subject to} \quad \lambda \geq 0 \quad (10b)$$

In order to obtain  $g(\lambda)$  and further solve (10), we apply primal decomposition to problem (9). Specifically we fix the coupling variable  $\tilde{t}$  and divide problem (9) into two levels. At the lower level, we have

$$\begin{aligned} & \underset{\tilde{P}, \tilde{T}, z}{\text{maximize}} && \tilde{t} - \lambda \left( \sum_{i \in S} e^{\tilde{T}_i} + \sum_{j \in R} e^{\tilde{T}_j} z_j - T_{frame} \right) && (11) \\ & \text{subject to} && (7b), (7d) - (7h) \end{aligned}$$

whose difference from problem (9) is that  $\tilde{t}$  is a constant for problem (11).

At the higher level we have the secondary master problem as

$$\underset{\tilde{t}}{\text{maximize}} \quad f^*(\tilde{t}, \lambda) \quad (12)$$

<sup>220</sup>  $f^*(\tilde{t}, \lambda)$  is the optimal value of problem (11) given  $\tilde{t}$  and  $\lambda$ . The result of (12) gives  $g(\lambda)$ .

Problem (11) can be decomposed into sub-problems that can be solved independently within each body region. For body region with node set  $G_k$ , the sub-problem is

$$\underset{\tilde{P}, \tilde{T}, z}{\text{maximize}} \quad -\lambda \left( \sum_{i \in S \cap G_k} e^{\tilde{T}_i} + \sum_{j \in R \cap G_k} e^{\tilde{T}_j} z_j \right) \quad (13a)$$

$$\text{subject to} \quad \tilde{t} + \tilde{P}_i + \tilde{T}_i \leq \ln(T_{frame} B_i), \quad i \in S \cap G_k \quad (13b)$$

$$\begin{aligned} & \tilde{T}_i + \ln \left( \sum_{j \in G_k \cap R} W \log \left( 1 + \frac{\alpha_{ij} e^{\tilde{P}_i}}{N_j} \right) z_j \right) \geq \ln(x_i T_{frame}) \\ & , \quad i \in G_k \cap S \end{aligned} \quad (13c)$$

$$\ln \left( \sum_{j \in G_k \cap R} r_{jc} e^{\tilde{T}_j} z_j \right) \geq \ln \left( \sum_{i \in G_k \cap S} x_i T_{frame} \right) \quad (13d)$$

$$\sum_{j \in G_k \cap R} z_j = 1 \quad (13e)$$

$$\tilde{P}_{\min} \leq \tilde{P}_i \leq \tilde{P}_{\max}, \quad i \in S \cap G_k \quad (13f)$$

$$z_j \in \{0, 1\}, \quad j \in R \cap G_k \quad (13g)$$

If we call the maximum value of sub-problem (13) as  $f_k^*(\tilde{t}, \lambda)$ , then  $f^*(\tilde{t}, \lambda) =$

$\tilde{t} + \lambda T_{frame} + \sum_{k=1}^6 f_k^*(\tilde{t}, \lambda)$ . Since only one relay can be selected in a certain body region, which results from the constraints (13e) and (13g), the above mixed integer sub-problem (13) can be solved by enumerating all possible values of  $z_j$  in this region. That is, we try each relay CS in that region and select the one that results in the optimal objective function value. With integer variable  $z_j$  obtained and removed, the sub-problem (13) becomes a regular convex optimization problem and can be solved efficiently. To further convert the problem so that it can be solved by CVX, which is one of the mostly used modeling system for convex optimization, (13c) is transformed into  $\tilde{T}_i + \ln \left( \sum_{j \in G_k \cap R} W \log \left( \frac{\alpha_{ij} e^{\tilde{P}_i}}{N_j} \right) z_j \right) \geq \ln(x_i T_{frame})$ . In our model, the condition  $\frac{\alpha_{ij} e^{\tilde{P}_i}}{N_j} \gg 1$  is ensured. The reason is that the sensors are only allowed to transmit to the relays in the same body region, which leads to a short communication distance. In our simulation, even with the lowest transmission power,  $\frac{\alpha_{ij} e^{\tilde{P}_i}}{N_j}$  is guaranteed to be above 40, which is much larger than 1. So the transformation for (13c) is reasonable and safe.

By solving each sub-problem, the optimal value for the binary decision variable  $z^*(\tilde{t}, \lambda)$  in problem (11) can be obtained.

Specifically, consider body region with node set  $G_k$ , if the  $j^{th}$  relay CS in this region achieves the highest value of (13a), then  $z_j = 1$  and  $z_l = 0$  for all  $l \neq j$ , where  $j, l \in R \cap G_k$ .

With  $z^*(\tilde{t}, \lambda)$  obtained, problem (11) can be transformed into

$$\underset{\tilde{P}, \tilde{T}}{\text{maximize}} \quad \tilde{t} - \lambda \left( \sum_{i \in S} e^{\tilde{T}_i} + \sum_{j \in R} e^{\tilde{T}_j} z_j^*(\tilde{t}, \lambda) - T_{frame} \right) \quad (14a)$$

$$\text{subject to} \quad \tilde{t} + \tilde{P}_i + \tilde{T}_i \leq \ln(T_{frame} B_i), \quad i \in S \quad (14b)$$

$$\begin{aligned} \tilde{T}_i + \ln \left( \sum_{j \in G_k \cap R} W \log \left( \frac{\alpha_{ij} e^{\tilde{P}_i}}{N_j} \right) z_j^*(\tilde{t}, \lambda) \right) &\geq \ln(x_i T_{frame}) \\ , \quad i \in G_k \cap S, \quad G_k \in G \end{aligned} \quad (14c)$$

$$\ln \left( \sum_{j \in G_k \cap R} r_{jc} e^{\tilde{T}_j} z_j^*(\tilde{t}, \lambda) \right) \geq \ln \left( \sum_{i \in G_k \cap S} x_i T_{frame} \right), \quad G_k \in G \quad (14d)$$

$$\tilde{P}_{\min} \leq \tilde{P}_i \leq \tilde{P}_{\max}, \quad i \in S \quad (14e)$$

It is worth noting that (14) is a convex problem.

In order to derive the gradient of  $f^*(\tilde{t}, \lambda)$  over  $\tilde{t}$  and conduct gradient ascent  
 245 method to obtain the solution of (12), the Lagrange dual function  $d(\gamma, \tilde{t}, \lambda)$  of  
 (14) is considered as

$$\begin{aligned} \underset{\tilde{P}, \tilde{T}}{\text{maximize}} \quad & \tilde{t} - \lambda \left( \sum_{i \in S} e^{\tilde{T}_i} + \sum_{j \in R} e^{\tilde{T}_j} z_j^*(\tilde{t}, \lambda) - T_{frame} \right) \\ & - \sum_{i \in S} \gamma_i \left( \tilde{t} + \tilde{P}_i + \tilde{T}_i - \ln(T_{frame} B_i) \right) \end{aligned} \quad (15)$$

$$\text{subject to} \quad (14c) - (14e)$$

The dual problem of (14) can be expressed as

$$\underset{\gamma}{\text{minimize}} \quad d(\gamma, \tilde{t}, \lambda) \quad (16a)$$

$$\text{subject to} \quad \gamma \geq 0 \quad (16b)$$

Because the optimal primal variables  $\tilde{P}^*(\tilde{t}, \lambda)$  and  $\tilde{T}^*(\tilde{t}, \lambda)$  of (14) are already  
 obtained and problem (14) is convex, the optimal solution  $\gamma^*(\tilde{t}, \lambda)$  of the dual

250 problem (16) can be derived according to the KKT conditions as is illustrated in the Appendix.

Since problem (14) is a convex problem, its duality gap with the dual problem (16) is zero and we have

$$\begin{aligned}
f^*(\tilde{t}, \lambda) &= \inf_{\gamma \geq 0} d(\gamma, \tilde{t}, \lambda) \\
&= \tilde{t} - \lambda \left( \sum_{i \in S} e^{\tilde{T}_i^*(\tilde{t}, \lambda)} + \sum_{j \in R} e^{\tilde{T}_j^*(\tilde{t}, \lambda)} z_j^*(\tilde{t}, \lambda) - T_{frame} \right) \\
&\quad - \sum_{i \in S} \gamma_i^*(\tilde{t}, \lambda) \left( \tilde{t} + \tilde{P}_i^*(\tilde{t}, \lambda) + \tilde{T}_i^*(\tilde{t}, \lambda) - \ln(T_{frame} B_i) \right) \quad (17)
\end{aligned}$$

where  $\tilde{T}^*(\tilde{t}, \lambda)$  and  $\tilde{P}^*(\tilde{t}, \lambda)$  are the optimal solutions of (14), and  $\gamma^*(\tilde{t}, \lambda)$  is the optimal solution of (16).

Thus the subgradient of  $f^*(\tilde{t}, \lambda)$  over  $\tilde{t}$  can be calculated as

$$\frac{\partial f^*(\tilde{t}, \lambda)}{\partial \tilde{t}} = 1 - \sum_{i \in S} \gamma_i^*(\tilde{t}, \lambda) \quad (18)$$

From (15), for each certain  $\gamma$ ,  $d(\gamma, \tilde{t}, \lambda)$  is an affine function of  $\tilde{t}$ . Since pointwise minimum preserves concavity,  $f^*(\tilde{t}, \lambda) = \inf_{\gamma \geq 0} d(\gamma, \tilde{t}, \lambda)$  is a concave function of  $\tilde{t}$  given  $\lambda$ . Thus (12) can be solved by subgradient ascent method using the updating rule for  $\tilde{t}$

$$\tilde{t} = \tilde{t} + \theta \left( 1 - \sum_{i \in S} \gamma_i^*(\tilde{t}, \lambda) \right) \quad (19)$$

Once the optimal value  $\tilde{t}^*(\lambda)$  is obtained,  $g(\lambda)$  can be calculated by

$$g(\lambda) = \tilde{t}^*(\lambda) - \lambda \left( \sum_{i \in S} e^{\tilde{T}_i^*(\tilde{t}^*(\lambda), \lambda)} + \sum_{j \in R} e^{\tilde{T}_j^*(\tilde{t}^*(\lambda), \lambda)} z_j^*(\tilde{t}^*(\lambda), \lambda) - T_{frame} \right) \quad (20)$$

For the same reason that  $f^*(\tilde{t}, \lambda)$  is a concave function of  $\tilde{t}$ ,  $g(\lambda)$  is a convex function of  $\lambda$ . The subgradient descent update for  $\lambda$  is

$$\lambda = \left[ \lambda + \theta \left( \sum_{i \in S} e^{\tilde{T}_i^*(\tilde{t}^*(\lambda), \lambda)} + \sum_{j \in R} e^{\tilde{T}_j^*(\tilde{t}^*(\lambda), \lambda)} z_j^*(\tilde{t}^*(\lambda), \lambda) - T_{frame} \right) \right]^+ \quad (21)$$

A flow chart of the proposed method is shown in Figure 4 and the pseudocode code is illustrated in Algorithm 1.

---

**Algorithm 1** Joint relay location control and cross-layer optimization algorithm

---

Initialize: step size  $\theta$ , threshold  $TH$ ,  $m = 1$ ,  $\lambda^0$  and  $\lambda^1$ .

**while**  $|\lambda^m - \lambda^{m-1}| \geq TH$  **do**

Initialize  $\tilde{t}^0, \tilde{t}^1, n = 1$ ;

**while**  $|\tilde{t}^n - \tilde{t}^{n-1}| \geq TH$  **do**

**for**  $G_k$  in each sub-region **do**

**for** each possible  $z_j, j \in G_k$  **do**

Solve the convex sub-problem (13);

**end for**

Obtain the optimal solutions given  $\tilde{t}^n, \lambda^m$ :  $z_k^*(\tilde{t}^n, \lambda^m), \tilde{P}_k^*(\tilde{t}^n, \lambda^m), \tilde{T}_k^*(\tilde{t}^n, \lambda^m)$ ;

**end for**

Obtain the optimal Lagrange multiplier  $\gamma^*(\tilde{t}^n, \lambda^m)$  of (14b) by KKT conditions;

$$\tilde{t}^{n+1} = \tilde{t}^n + \theta \frac{\partial f^*(\tilde{t}, \lambda^m)}{\partial \tilde{t}}, n = n + 1;$$

**end while**

$$\lambda^{m+1} = \lambda^m - \theta \frac{dg(\lambda)}{d\lambda}, m = m + 1;$$

**end while**

Return  $\tilde{P}^*(\tilde{t}^*(\lambda^*), \lambda^*), \tilde{T}^*(\tilde{t}^*(\lambda^*), \lambda^*), z^*(\tilde{t}^*(\lambda^*), \lambda^*), \lambda^*, \tilde{t}^*(\lambda^*), \gamma^*(\tilde{t}^*(\lambda^*), \lambda^*)$ .

---

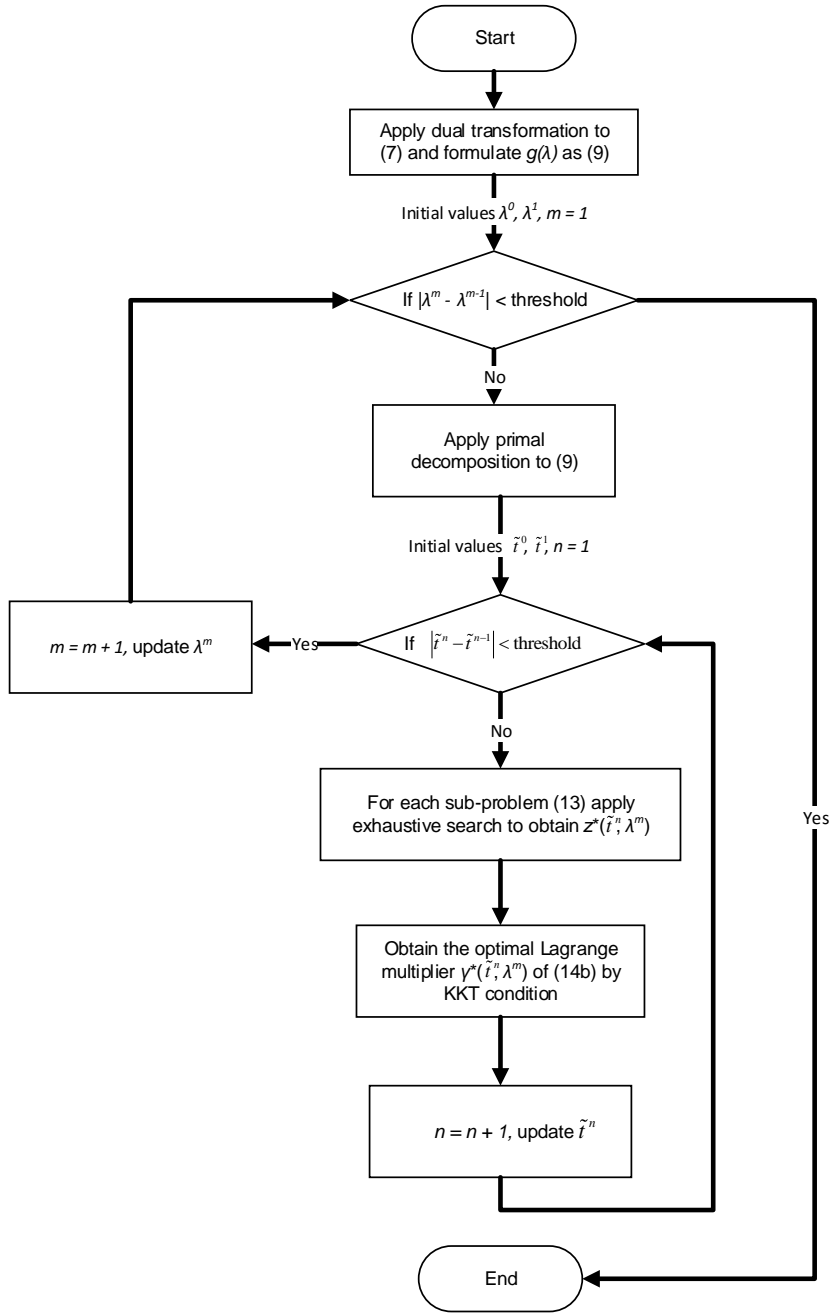


Figure 4: Flow chart

255 *4.2. Duality Gap*

In the proposed algorithm, dual decomposition is applied to the master problem (7), which is a non-convex problem. Thus the optimal solutions of the dual problem (10) formulated is potentially sub-optimal to the original problem proposed. There might be duality gap between the optimal values of the primal  
260 problem (7) and that of the dual problem (10).

To research on the influence of the duality gap, in the experiment section, we simulate a WBSN with small network size and obtain the optimal values of both primal problem (7) and dual problem (10). As will be illustrated in the simulation results in Section VI (Figure 8, Figure 9 and Figure 10), for the net-  
265 work we consider, the optimal network lifetime of the primal and dual problems are very close, which indicates the effectiveness of the proposed method.

### 5. Fast Convergence Rate Method Based on Binary Search

Generally speaking, the convergence rate of subgradient method is slow [25]. In this section, a solution based on binary search for the optimal values is  
270 proposed and achieves much faster convergence rate compared with pure sub-gradient method.

Consider the updating rules (19) and (21) for  $\tilde{t}$  and  $\lambda$ . Since it is known that  $f^*(\tilde{t}, \lambda)$  is a concave function of  $\tilde{t}$  and  $g(\lambda)$  is a convex function of  $\lambda$ , the convergence rate can be increased by observing the signs of the derivatives.

For  $\lambda$ , the curve of  $g(\lambda)$  can be illustrated as in Figure 5. Since  $\lambda$  is larger than or equal to zero, the lower bound  $\lambda_{Lower}$  is set to zero at the start. In order to find a proper upper bound, a step size  $\lambda_{Interval}$  is defined. The initial  $\lambda_{Upper}$  can be obtained by

$$\lambda_{Upper} = \lambda_{Lower} + N \times \lambda_{Interval} \quad (22)$$

275 where  $N$  is the smallest integer that satisfies  $\left. \frac{dg(\lambda)}{d\lambda} \right|_{\lambda=\lambda_{Upper}} > 0$ .

Once the initial upper bound and lower bound of  $\lambda$  are obtained, binary search for the optimal solution  $\lambda^*$  can be continued by checking the sign of the

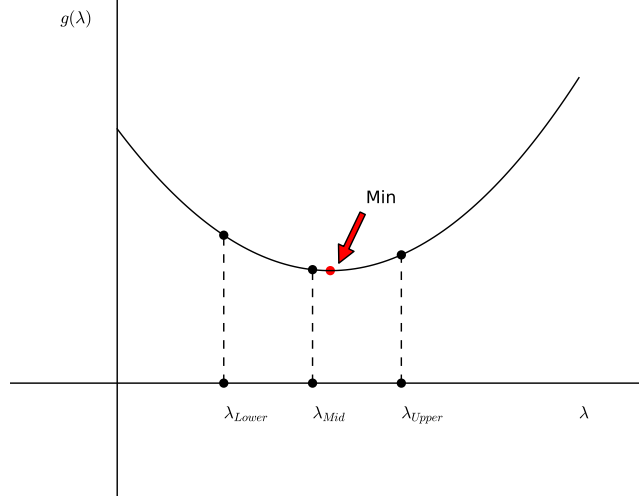


Figure 5: Binary search on optimal  $\lambda$

derivative at  $\lambda_{Mid} = \frac{\lambda_{Upper} + \lambda_{Lower}}{2}$  and updating the value of  $\lambda_{Upper}$  and  $\lambda_{Lower}$  iteratively.

280 For  $\tilde{t}$ , there is a threshold imposed by constraint (14b). When  $\tilde{t}$  grows too large, the problem (14) becomes infeasible. So there is a threshold  $\tilde{t}_{TH}$  for  $\tilde{t}$ , beyond which feasible  $\tilde{t}$  does not exist.  $f^*(\tilde{t}, \lambda)$  can be plotted as in Figure 6.

At the beginning, a  $\tilde{t}_{Lower}$  small enough and a proper  $\tilde{t}_{Interval}$  are chosen. The initial  $\tilde{t}_{Upper}$  can be derived by

$$\tilde{t}_{Upper} = \tilde{t}_{Lower} + N' \times \tilde{t}_{Interval} \quad (23)$$

where  $N'$  is the smallest integer that satisfies  $\left. \frac{df^*(\tilde{t}, \lambda)}{d\tilde{t}} \right|_{\tilde{t}=\tilde{t}_{Upper}} < 0$  or no solution exists for  $\tilde{t} = \tilde{t}_{Upper}$ .

285 The pseudocode for the proposed binary search algorithm is given in Algorithm 2.

---

**Algorithm 2** Proposed algorithm based on binary search
 

---

Initialize:  $\lambda_{Lower}$ ,  $\lambda_{Interval}$ , threshold  $TH$ .

Find  $\lambda_{Upper}$ ;

**while**  $\lambda_{Upper} - \lambda_{Lower} \geq TH$  **do**

$$\lambda_{Mid} = \frac{\lambda_{Upper} + \lambda_{Lower}}{2};$$

Initialize  $\tilde{t}_{Lower}$ ,  $\tilde{t}_{Interval}$  and find  $\tilde{t}_{Upper}$ ;

**while**  $\tilde{t}_{Upper} - \tilde{t}_{Lower} \geq TH$  **do**

$$\tilde{t}_{Mid} = \frac{\tilde{t}_{Upper} + \tilde{t}_{Lower}}{2} \text{ and calculate } \left. \frac{df^*(\tilde{t}, \lambda)}{d\tilde{t}} \right|_{\tilde{t}=\tilde{t}_{Mid}}$$

**if**  $\left. \frac{df^*(\tilde{t}, \lambda)}{d\tilde{t}} \right|_{\tilde{t}=\tilde{t}_{Mid}}$  does not exist **then**

$$\tilde{t}_{Upper} = \tilde{t}_{Mid};$$

**else if**  $\left. \frac{df^*(\tilde{t}, \lambda)}{d\tilde{t}} \right|_{\tilde{t}=\tilde{t}_{Mid}} < 0$  **then**

$$\tilde{t}_{Upper} = \tilde{t}_{Mid};$$

**else**

$$\tilde{t}_{Lower} = \tilde{t}_{Mid};$$

**end if**

**end while**

$$\tilde{t}^*(\lambda_{Mid}) = \frac{\tilde{t}_{Upper} + \tilde{t}_{Lower}}{2};$$

Obtain  $\tilde{P}^*(\tilde{t}^*(\lambda_{Mid}), \lambda_{Mid})$ ,  $\tilde{T}^*(\tilde{t}^*(\lambda_{Mid}), \lambda_{Mid})$ ,  $z^*(\tilde{t}^*(\lambda_{Mid}), \lambda_{Mid})$ ;

**if**  $\left. \frac{dg(\lambda)}{d\lambda} \right|_{\lambda=\lambda_{Mid}} > 0$  **then**

$$\lambda_{Upper} = \lambda_{Mid};$$

**else**

$$\lambda_{Lower} = \lambda_{Mid};$$

**end if**

**end while**

$$\lambda^* = \frac{\lambda_{Upper} + \lambda_{Lower}}{2};$$

Return  $\tilde{P}^*(\tilde{t}^*(\lambda^*), \lambda^*)$ ,  $\tilde{T}^*(\tilde{t}^*(\lambda^*), \lambda^*)$ ,  $z^*(\tilde{t}^*(\lambda^*), \lambda^*)$ ,  $\lambda^*$ ,  $\tilde{t}^*(\lambda^*)$ ,

$\gamma^*(\tilde{t}^*(\lambda^*), \lambda^*)$ .

---

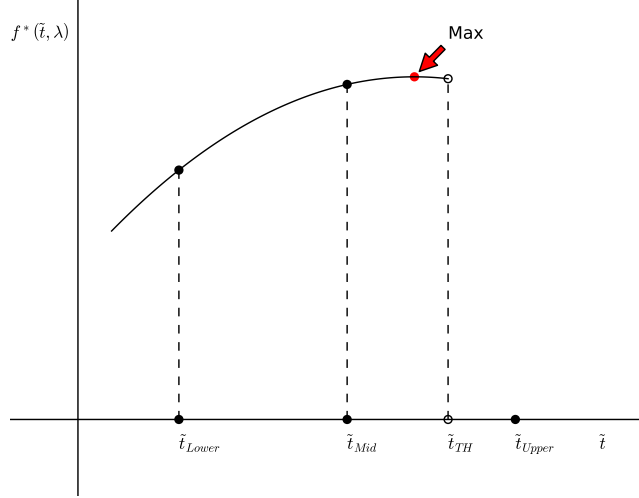


Figure 6: Binary search on optimal  $\tilde{t}$

## 6. Simulation Results

### 6.1. System Settings

We assume there are 17 implanted sensor nodes and 40 relay CSs in the  
 290 Wireless In-Body Sensor Network that we consider. The sensor nodes and relay  
 CSs are placed as is shown in Figure 2a. The initial battery level of the sensor  
 nodes are set to be 1J. The maximum transmission power is  $P_{max} = 0\text{dBm}$  and  
 the minimum is  $P_{min} = -15\text{dBm}$ . A typical noise density value  $-174\text{dBm/Hz}$  is  
 used. According to IEEE standard 802.15.6 [23], the transceivers of body sensor  
 295 networks work at frequency band 402MHz-405MHz and there are 10 channels.  
 In the simulation, only one channel is used and the bandwidth  $W = 0.3\text{MHz}$ .

The path loss in dB at distance  $d$  with reference distance  $d_0$  can be calculated  
 as

$$PL(d) = PL(d_0) + 10n \log\left(\frac{d}{d_0}\right) \quad (24)$$

For in-body channels between the implanted sensors and the on-body relays,  
 we use the channel model parameters from [26]. The reference distance  $d_0$  is

5cm. Path loss at the reference location is 47.14dB and the path loss exponent  $n$  is 4.26. For on-body channels between the relays and the coordinator, channel model parameters from [27] are applied. The reference distance  $d_0$  is 10cm. Path loss at the reference location is 35.20dB and the path loss exponent  $n$  is 3.11.

To evaluate the proposed algorithm, multi-hop network with only transmission power control as in [20] and multi-hop network with only relay location optimization as in [18] are used as comparisons. In the multi-hop network with only transmission power control and no relay location optimization, one relay CS is selected randomly within each body region and is used to relay the messages of the implanted sensors in that region. For the multi-hop network with only relay location control, the transmission power for each sensor node is set to be -10dBmW.

Furthermore, in order to check the duality gap between the primal problem (7) and the dual problem (10), the optimal network lifetime from solving the centralized problem (7) directly is also plotted. Problem (7) is solved by enumerating all possible values of  $z$  directly and selecting the  $z$  value that results in the maximum objective value (7a). It is worth noting that the reason problem (7) can be solved directly using a centralized method is that we assume a small number of relay CSs in the simulation. As the number of relay CSs increases, the number of the cases to enumerate for variable  $z$  in the centralized solution will increase with a power of 6 according to (7f) and (7h). The running time for the centralized method can become unreasonably long very easily. For example, if the number of relay CSs is doubled in each body region, the running time for the centralized solution will become  $2^6$  times as much as that of the original problem. For comparison, the running time for the proposed decomposition method only increases linearly to the number of relay CSs according to sub-problem (13).

The optimization problems are solved by CVX 2.1 with Mosek solver in Windows/64-X86 environment. The platform is equipped with Xeon(R) processor with 4 cores and the operating frequency is 3.5GHz.

Figure 7 shows a typical result of the optimal network topology and data flow. The data rate for each sensor is 40Kbps and the superframe length is 400ms. The black lines represent the optimal traffic paths among the in-body sensors, the on-body relays and the coordinator. The thickness of the lines is proportional to the channel capacity.

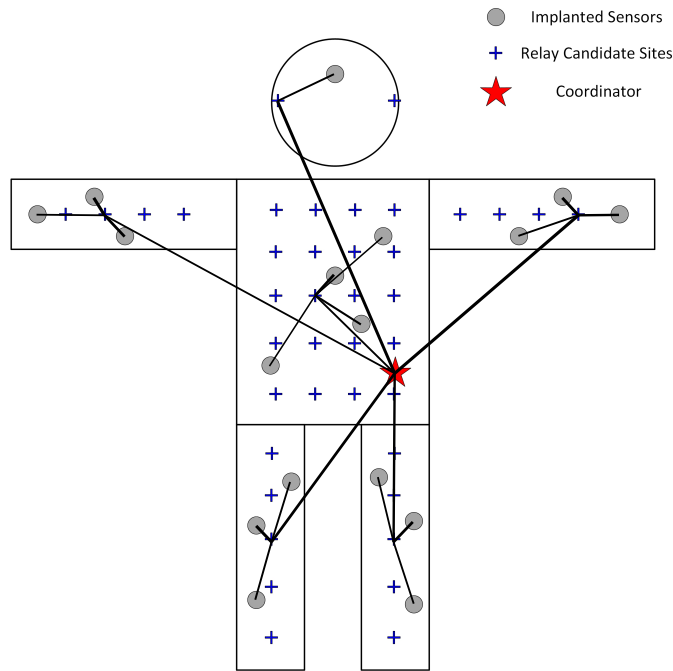


Figure 7: The optimal network topology and channel capacity

### 6.2.1. The influence of the traffic generated by sensors

The influence of the traffic generated by sensors on the network lifetime is shown in Figure 8. It is assumed that all sensors generate data streams with the same speed. The superframe length  $T_{frame}$  is set to be 400ms. The proposed network optimization method, which jointly considers the relay location control and network cross-layer optimization, achieves much longer network lifetime

than the alternatives. Specifically, compared with the other multi-hop networks simulated, the proposed network achieves around 20% longer network lifetime. As data rate increases, the energy consumption per superframe grows larger and the sensors' energy is consumed faster. So the network lifetime becomes shorter  
345 when traffic of the sensors becomes larger as is illustrated in Figure 8.

It is worth noting that when the data rate for each sensor node is higher than 40Kbps, the network with fixed transmission power fails to provide feasible solutions. When the data rate for each sensor node is higher than 45Kbps,  
350 the network without relay location optimization is unable to provide feasible solutions. The reason is that these two methods search over a smaller feasible set compared with the proposed approach. In this way, even when the average traffic for the sensor nodes grows to around 50Kbps, the proposed approach is still able to guarantee that all sensors finish their transmissions within  $T_{frame}$   
355 without collisions and provides feasible solutions.

From Figure 8, it can be further concluded that compared with solving the centralized problem (7) directly, the proposed decomposition method yields the optimal network lifetime values that are very close. So the duality gap between the optimal values of problem (7) and (10) is trivial and the solution of the dual  
360 problem (10) is a good approximation to that of the primal problem (7).

The gap between the results of the network without relay location optimization and that of the proposed network grows larger when traffic of the sensors increases. The reason is that when the sensors' data rate is high, the optimal transmission power approaches to the maximum value and power control  
365 becomes less helpful. The effect of relay location optimization becomes more profound.

### 6.2.2. *The influence of the number of sensors*

The optimal network lifetime of deploying different number of sensors are plotted in Figure 9. The traffic generated by each sensor is set to be 40Kbps  
370 and the superframe length is set to be 400ms. There are originally 17 sensors as in Figure 2a and we consider the influence of removing some of the sensors.

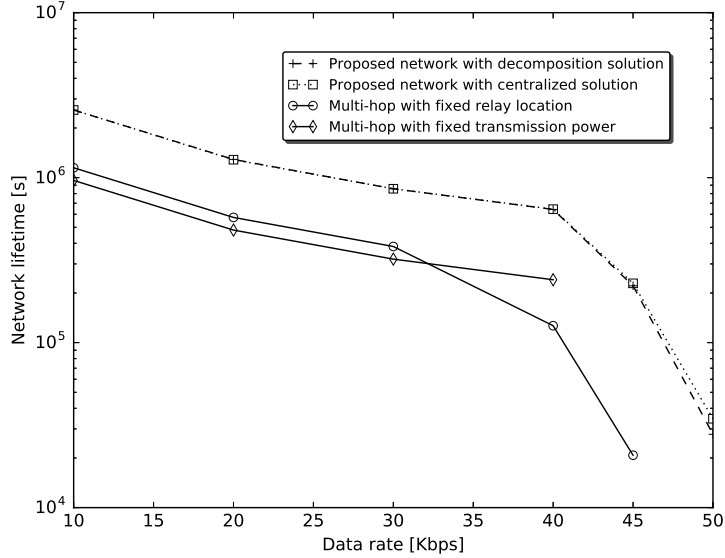


Figure 8: The influence of the traffic generated by sensors

Though the sequence of removing or adding the sensors can influence the final results, the characteristics exhibited stay the same. As is shown in Figure 9, the proposed network optimization method yields the highest network lifetime, which is consistent with the previous results.

It is worth noting that the curves exhibit step shape. For example, when the number of the sensor nodes increases from 11 to 12, there is an obvious network lifetime decrease for all curves. Around this decrease, the values of the curves remain stable. In our experiment, this is when the 12<sup>th</sup> sensor node is added to the torso and a new “bottleneck” node shows up. Here the “bottleneck” indicates the sensor node with the lowest lifetime value in the network, which equals to the value of the whole network’s lifetime. If the number of sensors becomes large, because the total time for the transmissions in a round is limited and constrained according to (4b), the transmission power of the sensors needs to be improved to transmit faster and meet the time constraint. The energy

spent in each superframe for each node can be calculated as

$$E_i = T_i P_i = \frac{x_i T_{frame}}{r_{ij}} P_i = \frac{x_i T_{frame}}{W \log \left( 1 + \frac{\alpha_{ij} P_i}{N_j} \right)} P_i \quad (25)$$

so the higher the transmission power is, the higher energy consumption will be in each superframe and the lifetime of the sensor nodes will decrease.

Since the objective of the optimization problem is to maximize the shortest sensor lifetime, when a new sensor is added, the bottleneck sensor will not be affected if it is possible to add the new sensor and only decrease the non-bottleneck sensors' lifetime. So during the process of adding more sensors, we are expected to see, when only non-bottleneck sensors' lifetime is shortened and the bottleneck sensor's lifetime remains the same, the network lifetime does not change. Only when the lifetime of all sensors are close enough, after adding a new sensor, a new bottleneck sensor appears and the network lifetime decreases. This is the reason why step shaped curves show up.

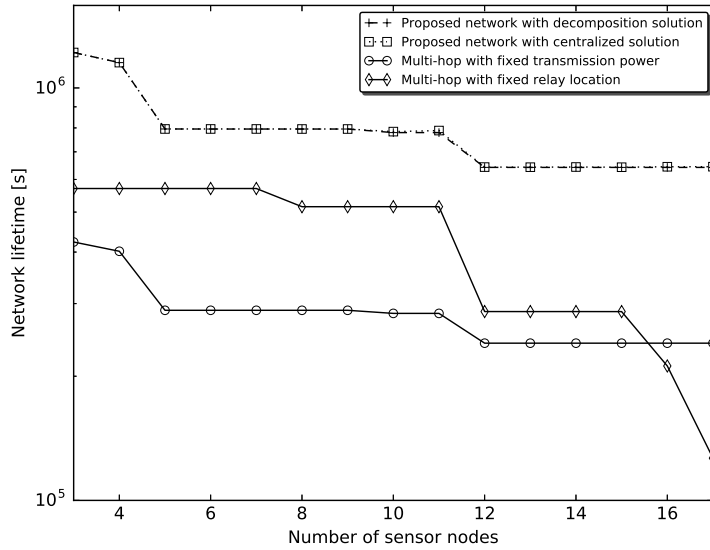


Figure 9: The influence of the number of sensors

### 6.2.3. Energy consumption comparison

Figure 10 shows the total network energy consumption in each superframe of the methods considered. The proposed network optimization approach achieves the lowest energy consumption, which is consistent with the analysis of the network lifetime. The results of the proposed decomposition solution and centralized solution are still almost identical. When traffic of each node is larger than 40Kbps, the energy consumption of all methods grows up sharply, which coincides with the results of network lifetime in Figure 8. From Figure 8, it can be seen that the network lifetime decreases fast when data rate is beyond 40Kbps.

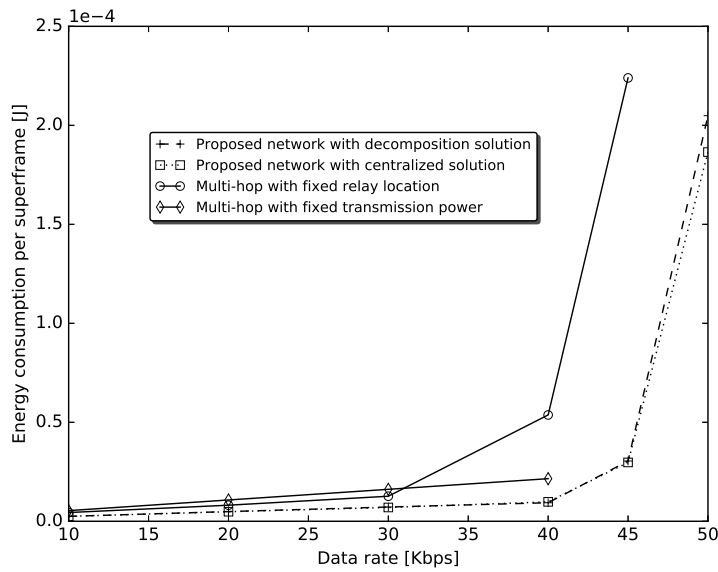


Figure 10: Energy consumption comparison

### 6.2.4. Lifetime of the sensor nodes

Figure 11 shows the lifetime of all sensor nodes derived from the proposed decomposition method. The sensor indexes are the same as in Figure 2a. Still the traffic for each sensor is 40Kbps and the superframe length is 400ms. From

Figure 11, it can be concluded that the lifetime results of the sensors in different regions are quite even. This indicates that no body region is the bottleneck of the whole network’s lifetime. If the network lifetime is to be increased, more relays need to be added to all regions at the same time.

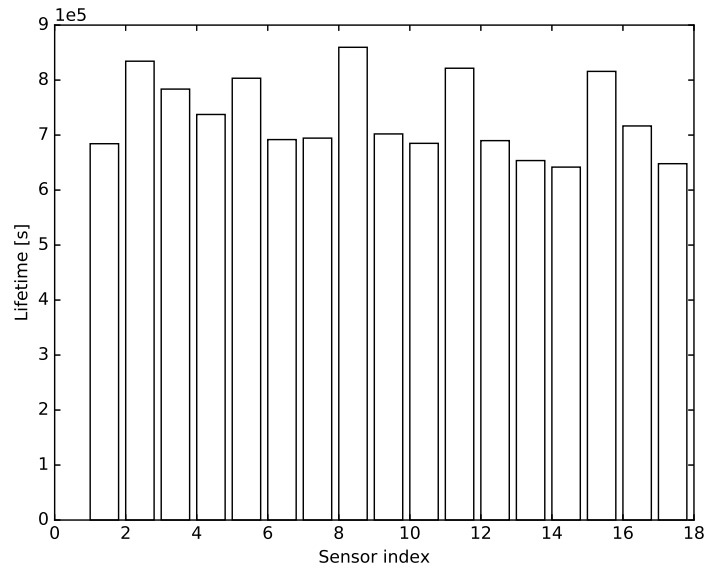


Figure 11: Lifetime of the sensors

405 *6.2.5. The influence of the number of relays*

Here we provide a brief discussion on how the number of relays influences the network lifetime. If the number of relays is increased, the sensor node with a short lifetime, especially the “bottleneck” sensor node, has the chance to select a nearer relay, thus saves its energy and live longer. In this way, the network  
 410 lifetime is expected to increase.

In the simulation, there are originally 6 relays as in Figure 7 and we choose to add relays to the body regions evenly. The number of relays on the head is kept to be one since there is only one sensor node and the network lifetime will not be influenced by adding more relays there. Each sensor node will choose the nearest  
 415 relay that is in the same region. In this section, we only provide the results of

the proposed decomposition method based on binary search. The reason is that when it is allowed to choose more than one relays in each body region, the number of occasions to enumerate in the centralized method grows very fast as mentioned previously. The amount of time consumed to solve the centralized  
 420 problem soon becomes unreasonable. In comparison, the time consumed by the decomposition method grows much slower with the increase of relay number.

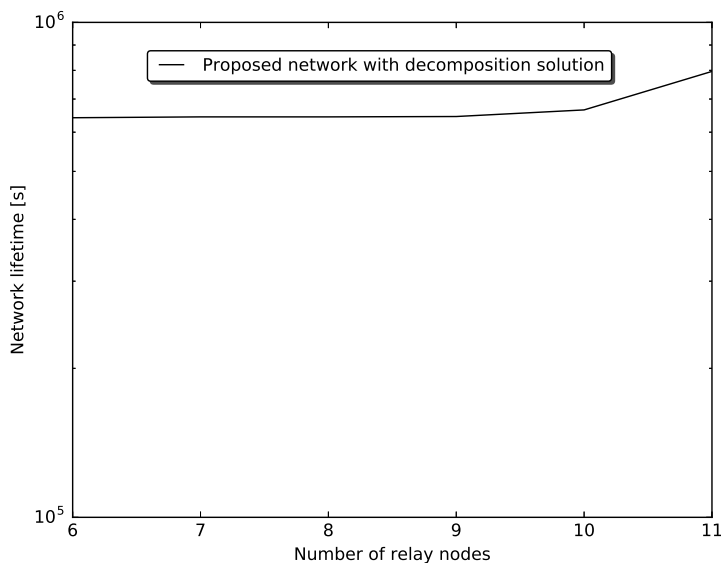


Figure 12: The influence of the number of relays

As is shown in Figure 12, the largest increase of the network lifetime happens between the 10<sup>th</sup> and the 11<sup>th</sup> relay, before which the network lifetime only increases moderately. This observation can be explained by the results shown  
 425 in Figure 11. In Figure 11 there are 6 relays, and for each region, there is some sensor node whose lifetime is almost as low as that of the bottleneck sensor node. That is to say, in order to increase the whole network lifetime, more relays should be added to nearly all the regions, so that each of these short-lived sensors are tackled and their lifetimes are prolonged. Before that, the  
 430 network lifetime only increases moderately as the number of relays grows.

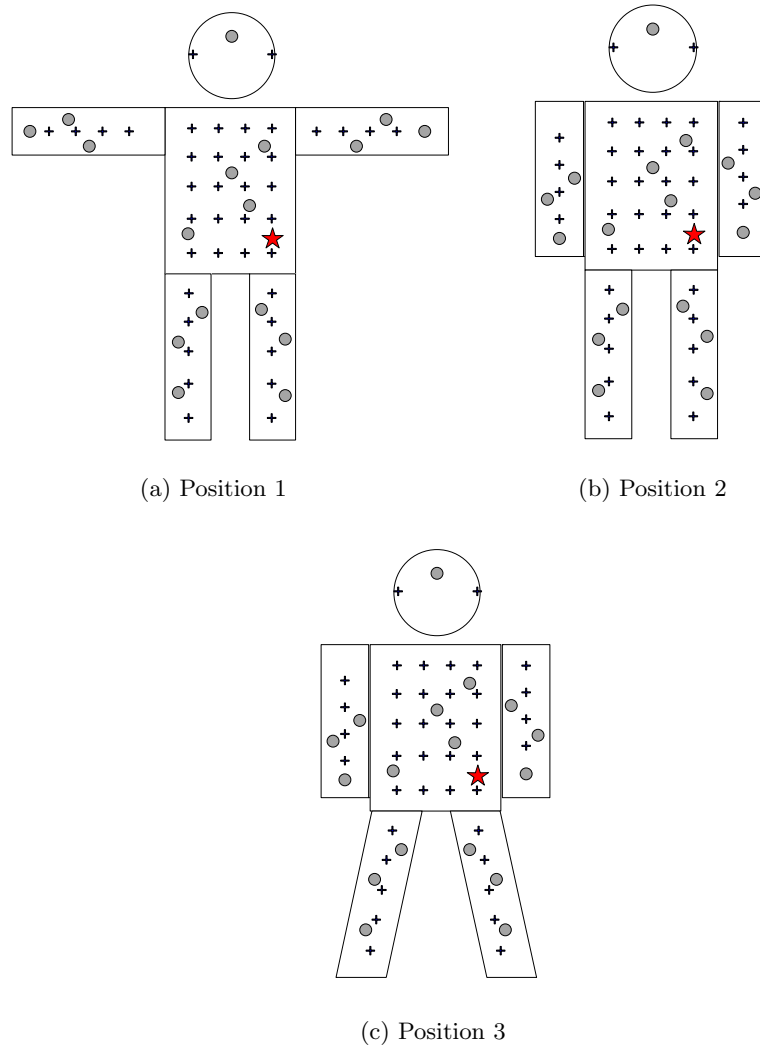


Figure 13: Three different standing positions in the simulation

### 6.2.6. The influence of body gesture

Body gesture change is one of the key features that distinguish WBSN from other general WSNs. In order to look into the influence of body movement on the network performance, we conduct simulation on three different standing positions as shown in Figure 13. According to the analysis in Section III,

Table 2: Network lifetime [s] results for three body positions

		10Kbps	20Kbps	30Kbps	40Kbps	45Kbps	50Kbps
Position 1	Proposed decomposition	2.56923e+06	1.29017e+06	8.56168e+05	6.41688e+05	2.21018e+05	2.78254e+04
	Proposed centralized	2.57099e+06	1.28446e+06	8.56446e+05	6.44264e+05	2.28773e+05	3.45601e+04
	Fixed relay location	1.14800e+06	5.73944e+05	3.82667e+05	1.26615e+05	2.07722e+04	NaN
	Fixed transmission power	9.62167e+05	4.81084e+05	3.20722e+05	2.40542e+05	NaN	NaN
Position 2	Proposed decomposition	2.56655e+06	1.28378e+06	8.55537e+05	6.41629e+05	3.06432e+05	5.37266e+04
	Proposed centralized	2.56864e+06	1.28457e+06	8.56274e+05	6.42574e+05	3.16206e+05	5.87761e+04
	Fixed relay location	1.14799e+06	5.74002e+05	3.82592e+05	1.35012e+05	2.79811e+04	NaN
	Fixed transmission power	9.62167e+05	4.81084e+05	3.20722e+05	2.40542e+05	2.13815e+05	NaN
Position 3	Proposed decomposition	2.56655e+06	1.28320e+06	8.55537e+05	6.41628e+05	1.87684e+05	3.38611e+04
	Proposed centralized	2.56903e+06	1.28532e+06	8.56575e+05	6.42618e+05	2.24166e+05	3.84971e+04
	Fixed relay location	1.14785e+06	5.73218e+05	3.82615e+05	1.05530e+05	NaN	NaN
	Fixed transmission power	9.62167e+05	4.81084e+05	3.20722e+05	2.40542e+05	NaN	NaN

by dividing body into several body regions, the relative distances between the sensors and relays are kept stable and the influence of body position change on network performance should be alleviated.

The simulation results are shown in Table 2 with average data generation rate  
440 for each sensor as an independent variable. The network lifetimes in seconds for each data rate and scenario composition are listed. “NaN” represents no feasible solution is found. The proposed model provides consistently better network lifetime performance than the rest two alternative models. From the table, it can be concluded that when data rate is low, the performance of different body  
445 positions are very close. When data rate is higher, body gesture change results in more obvious influence on the lifetime performance. The proposed model with both decomposition and centralized methods are able to find feasible solutions for all the data rates that are researched in the simulation. However, the rest two comparisons often fail to find feasible solutions when data rate is high.

450 6.2.7. Running time comparison

As is shown in Figure 14, in the simulation, the decomposition algorithm based on binary search consumes less time compared with the other methods. The rectangular bars represent the average values and the line segments on the top represent the value range of one standard deviation. The decomposition method based on subgradient descent/ascent approach is time consuming and binary search is able to expedite the running process greatly. The centralized approach requires about twice as much running time compared with the binary search method. As is shown by the figure, the decomposition methods are influenced by the initial values of the parameters, so the running time varies for different runs a lot. In contrast, the centralized method has a more stable running time. However, it is worth noting that when the number of relay CSs becomes larger, the running time consumed by the centralized method grows much faster than that of the decomposition method.

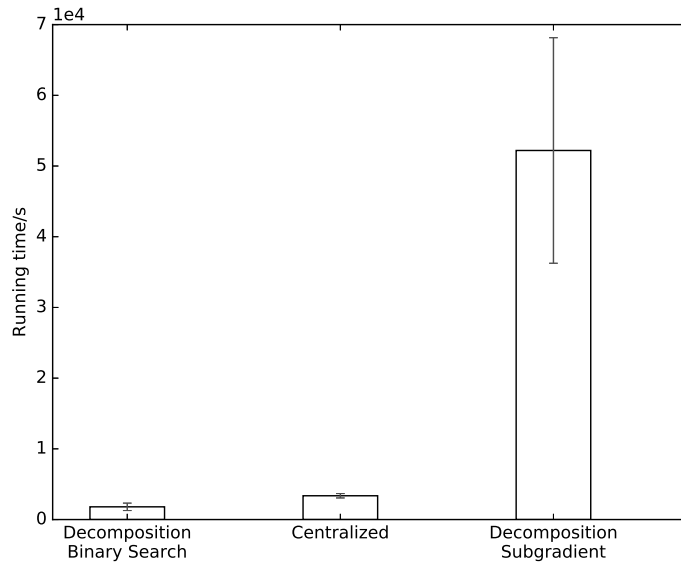


Figure 14: Running time comparison

## 7. Conclusion

465 In this article, we propose a network optimization approach that jointly  
 considers the relay location control and network cross-layer optimization, which  
 is suitable for the WBSN context. Multilevel primal and dual decomposition  
 methods are proposed to transform the original non-convex problem into convex  
 ones, which can be solved by CVX solvers. To expedite the running process of  
 470 optimization, an effective binary search approach is proposed. According to the  
 simulation results, compared with the literature, the proposed decomposition  
 method yields clear improvements on the network performances.

## Appendix

Since problem (14) is convex and apparently Slater condition can be satisfied,  
 thus strong duality holds. The optimal value of the Lagrange multiplier of  
 (14b) can be derived by first forming the Lagrangian including all inequality  
 constraints of problem (14) as

$$\begin{aligned}
 & L(\gamma, \eta, \nu, \omega, \tau, \tilde{P}, \tilde{T}) \\
 &= \tilde{t} - \lambda \left( \sum_{i \in S} e^{\tilde{T}_i} + \sum_{i \in R} e^{\tilde{T}_i} z_j^* \right) \\
 &\quad - \sum_{i \in S} \gamma_i \left( \tilde{t} + \tilde{P}_i + \tilde{T}_i - \ln(T_{frame} B_i) \right) \\
 &\quad - \sum_{i \in S} \eta_i \left( \ln(x_i T_{frame}) - \left( \tilde{T}_i + \ln \left( \sum_{j \in G_k \cap R, G_k \ni i} W \log \left( \frac{\alpha_{ij} e^{\tilde{P}_i}}{N_j} \right) z_j^* \right) \right) \right) \\
 &\quad - \sum_{G_k \in G} \nu_k \left( \ln \left( \sum_{i \in G_k \cap S} x_i T_{frame} \right) - \ln \left( \sum_{j \in G_k \cap R} r_{jc} e^{\tilde{T}_j} z_j^* \right) \right) \\
 &\quad - \sum_{i \in S} \omega_i \left( \tilde{P}_i - \tilde{P}_{\max} \right) \\
 &\quad - \sum_{i \in S} \tau_i \left( \tilde{P}_{\min} - \tilde{P}_i \right)
 \end{aligned}$$

Then according to the KKT conditions

$$\begin{aligned}
& \tilde{t} + \tilde{P}_i + \tilde{T}_i - \ln(T_{frame}B_i) \leq 0, \quad i \in S \\
& \ln(x_i T_{frame}) \leq \tilde{T}_i + \ln\left(\sum_{j \in G_k \cap R} W \log\left(\frac{\alpha_{ij} e^{\tilde{P}_i}}{N_j}\right) z_j^*\right), \quad i \in G_k \cap S, G_k \in G \\
& \ln\left(\sum_{i \in G_k \cap S} x_i T_{frame}\right) \leq \ln\left(\sum_{j \in G_k \cap R} r_{jc} e^{\tilde{T}_j} z_j^*\right), \quad G_k \in G \\
& \tilde{P}_i - \tilde{P}_{\max} \leq 0, \quad \tilde{P}_{\min} - \tilde{P}_i \leq 0, \quad i \in S \\
& \gamma \geq 0, \quad \eta \geq 0, \quad \nu \geq 0, \quad \omega \geq 0, \quad \tau \geq 0 \\
& \gamma_i (\tilde{t} + \tilde{P}_i + \tilde{T}_i - \ln(T_{frame}B_i)) = 0, \quad i \in S \\
& \eta_i \ln(x_i T_{frame}) = \eta_i \left( \tilde{T}_i + \ln\left(\sum_{j \in G_k \cap R, G_k \ni i} W \log\left(\frac{\alpha_{ij} e^{\tilde{P}_i}}{N_j}\right) z_j^*\right) \right), \quad i \in S \\
& \nu_k \left( \ln\left(\sum_{i \in G_k \cap S} x_i T_{frame}\right) - \ln\left(\sum_{j \in G_k \cap R} r_{jc} e^{\tilde{T}_j} z_j^*\right) \right) = 0, \quad G_k \in G \\
& \omega_i (\tilde{P}_i - \tilde{P}_{\max}) = 0, \quad i \in S \\
& \tau_i (\tilde{P}_{\min} - \tilde{P}_i) = 0, \quad i \in S \\
& \frac{\partial L}{\partial \tilde{P}_i} = -\gamma_i + \eta_i \frac{\log e}{\log\left(\frac{\alpha_{ij}}{N_j}\right) + \tilde{P}_i \log e} - \omega_i + \tau_i, \quad i \in S, j \in G_k \cap R, G_k \ni i, z_j^* = 1 \\
& \frac{\partial L}{\partial \tilde{T}_i} = -\lambda e^{\tilde{T}_i} - \gamma_i + \eta_i, \quad i \in S \\
& \frac{\partial L}{\partial \tilde{T}_j} = -\lambda e^{\tilde{T}_j} + \nu_k, \quad z_j^* = 1, \quad j \in G_k
\end{aligned}$$

the optimal solution  $\gamma^*(\tilde{t}, \lambda)$  can be solved given  $\tilde{P}^*(\tilde{t}, \lambda)$  and  $\tilde{T}^*(\tilde{t}, \lambda)$ , which  
475 are derived from solving the convex problem (14) directly.

### Acknowledgment

This work was supported by the Canadian Natural Sciences and Engineering Research Council.

## References

- 480 [1] L. Liu, L. Liu, P. D. Doncker, C. Oestges, Fading correlation measurement and modeling on the front side of a human body, EuCAP 2009.
- [2] W. G. Scanlon, S. L. Cotton, Understanding on-body fading channels at 2.45 ghz using measurements based on user state and environment, in: Antennas and Propagation Conference, 2008. LAPC 2008. Loughborough, IEEE, 2008, pp. 10–13.
- 485 [3] Y. Zhao, Y. Hao, A. Alomainy, C. Parini, Uwb on-body radio channel modeling using ray theory and subband fdtd method, Microwave Theory and Techniques, IEEE Transactions on 54 (4) (2006) 1827–1835.
- [4] D. R. B. G. J. D. D. Smith, L. Hanlen, V. Chaganti, Body area network radio channel measurement set, [http://filestore.nicta.com.au/Comms/OpenNICTA/NICTA\\_BodyAreaNetwork\\_RadioChannel\\_Data/](http://filestore.nicta.com.au/Comms/OpenNICTA/NICTA_BodyAreaNetwork_RadioChannel_Data/), accessed 10-Dec-2015.
- 490 [5] R. Chavez-Santiago, K. Sayrafian-Pour, A. Khaleghi, K. Takizawa, J. Wang, I. Balasingham, H.-B. Li, Propagation models for ieee 802.15.6 standardization of implant communication in body area networks, Communications Magazine, IEEE 51 (8) (2013) 80–87.
- 495 [6] G. E. Santagati, T. Melodia, U-wear: Software-defined ultrasonic networking for wearable devices, in: Proceedings of the 13th Annual International Conference on Mobile Systems, Applications, and Services, ACM, 2015, pp. 241–256.
- 500 [7] G. E. Santagati, T. Melodia, Experimental evaluation of impulsive ultrasonic intra-body communications for implantable biomedical devices.
- [8] A. L. Stolyar, Maximizing queueing network utility subject to stability: Greedy primal-dual algorithm, Queueing Systems 50 (4) (2005) 401–457.

- 505 [9] X. Lin, N. B. Shroff, Joint rate control and scheduling in multihop wireless networks, in: Decision and Control, 2004. CDC. 43rd IEEE Conference on, Vol. 2, IEEE, 2004, pp. 1484–1489.
- [10] X. Lin, N. B. Shroff, The impact of imperfect scheduling on cross-layer rate control in wireless networks, in: INFOCOM 2005. 24th Annual Joint Conference of the IEEE Computer and Communications Societies. Proceedings IEEE, Vol. 3, IEEE, 2005, pp. 1804–1814.  
510
- [11] A. Eryilmaz, R. Srikant, Fair resource allocation in wireless networks using queue-length-based scheduling and congestion control, in: INFOCOM 2005. 24th Annual Joint Conference of the IEEE Computer and Communications Societies. Proceedings IEEE, Vol. 3, IEEE, 2005, pp. 1794–1803.  
515
- [12] A. Eryilmaz, R. Srikant, Joint congestion control, routing, and mac for stability and fairness in wireless networks, Selected Areas in Communications, IEEE Journal on 24 (8) (2006) 1514–1524.
- [13] M. Johansson, L. Xiao, Scheduling, routing and power allocation for fairness in wireless networks, in: Vehicular Technology Conference, 2004. VTC 2004-Spring. 2004 IEEE 59th, Vol. 3, IEEE, 2004, pp. 1355–1360.  
520
- [14] Z. Sheng, Z. Ding, K. K. Leung, Distributed and power efficient routing in wireless cooperative networks, in: 2009 IEEE International Conference on Communications, IEEE, 2009, pp. 1–5.
- 525 [15] A. Boulis, D. Smith, D. Miniutti, L. Libman, Y. Tselishchev, Challenges in body area networks for healthcare: The mac, Communications Magazine, IEEE 50 (5) (2012) 100–106.
- [16] M. Momoda, S. Hara, A cooperative relaying scheme for real-time vital data gathering in a wearable wireless body area network, in: Medical Information and Communication Technology (ISMICT), 2013 7th International Symposium on, IEEE, 2013, pp. 38–41.  
530

- [17] J. Dong, D. Smith, Joint relay selection and transmit power control for wireless body area networks coexistence, in: Communications (ICC), 2014 IEEE International Conference on, IEEE, 2014, pp. 5676–5681.
- 535 [18] J. Elias, A. Mehaoua, Energy-aware topology design for wireless body area networks, in: Communications (ICC), 2012 IEEE International Conference on, IEEE, 2012, pp. 3409–3410.
- [19] X. Zhou, T. Zhang, L. Song, Q. Zhang, Energy efficiency optimization by resource allocation in wireless body area networks, in: Vehicular Technology Conference (VTC Spring), 2014 IEEE 79th, IEEE, 2014, pp. 1–6.
- 540 [20] N. Javaid, A. Ahmad, Y. Khan, Z. A. Khan, T. A. Alghamdi, A relay based routing protocol for wireless in-body sensor networks, *Wireless Personal Communications* 80 (3) (2015) 1063–1078.
- [21] R. R. Boorstyn, H. Frank, Large-scale network topological optimization, Communications, *IEEE Transactions on* 25 (1) (1977) 29–47.
- 545 [22] S. Movassaghi, M. Abolhasan, J. Lipman, A review of routing protocols in wireless body area networks, *Journal of Networks* 8 (3) (2013) 559–575.
- [23] A. Astrin, et al., Ieee standard for local and metropolitan area networks part 15.6: Wireless body area networks: Ieee std 802.15. 6-2012, The document is available at IEEE Xplore.
- 550 [24] R. Madan, S. Lall, Distributed algorithms for maximum lifetime routing in wireless sensor networks, *Wireless Communications, IEEE Transactions on* 5 (8) (2006) 2185–2193.
- [25] N. Z. Shor, *Minimization methods for non-differentiable functions*, Vol. 3, Springer Science & Business Media, 2012.
- 555 [26] K. Sayrafian-Pour, W.-B. Yang, J. Hagedorn, J. Terrill, K. Y. Yazdandoost, K. Hamaguchi, Channel models for medical implant communication, *International Journal of Wireless Information Networks* 17 (3-4) (2010) 105–112.

- [27] E. Reusens, W. Joseph, B. Latré, B. Braem, G. Vermeeren, E. Tanghe,  
560 L. Martens, I. Moerman, C. Blondia, Characterization of on-body communication channel and energy efficient topology design for wireless body area networks, *Information Technology in Biomedicine*, IEEE Transactions on 13 (6) (2009) 933–945.